nature materials

LETTERS

PUBLISHED ONLINE: 8 AUGUST 2016 | DOI: 10.1038/NMAT4722

A sub-femtojoule electrical spin-switch based on optically trapped polariton condensates

Alexander Dreismann[1], Hamid Ohadi[1], Yago del Valle-Inclan Redondo[1], Ryan Balili[1], Yuri G. Rubo[2], Simeon I. Tsintzos[3], George Deligeorgis[4], Zacharias Hatzopoulos[3,4], Pavlos G. Savvidis[1,4,5] and Jeremy J. Baumberg[1]*

Practical challenges to extrapolating Moore's law favour alternatives to electrons as information carriers. Two promising candidates are spin-based and all-optical architectures, the former offering lower energy consumption[1], the latter superior signal transfer down to the level of chip-interconnects[2]. Polaritons—spinor quasi-particles composed of semiconductor excitons and microcavity photons—directly couple exciton spins and photon polarizations, combining the advantages of both approaches. However, their implementation for spintronics has been hindered because polariton spins can be manipulated only optically[3,4] or by strong magnetic fields[5,6]. Here we use an external electric field to directly control the spin of a polariton condensate, bias-tuning the emission polarization. The nonlinear spin dynamics offers an alternative route to switching, allowing us to realize an electrical spin-switch exhibiting ultralow switching energies below 0.5 fJ. Our results lay the foundation for development of devices based on the electro-optical control of coherent spin ensembles on a chip.

Polaritons result from strong coupling of quantum-well (QW) excitons and photons in semiconductor microcavities. Their properties are determined by their constituents: from their photonic fraction comes a small effective mass ($\sim 10^{-4} m_e$) and propagation over long distances at high speeds, while their excitonic component imparts strong self-interactions, resulting in large nonlinearities[7,8]. These characteristics favour Bose-stimulated condensation into macroscopic quantum states, fully coherent light–matter waves that spread over tens of micrometres and manifest a number of properties resembling atomic Bose–Einstein condensates and superfluids[9–11]. A number of polariton-based devices have been reported in the literature, including ultralow-power all-optical transistors and switches[12,13].

Polaritons have two spin projections $s_z = \pm 1$ arising from the coupling between spin-up (-down) heavy-hole excitons and right-(left-)circularly polarized photons[3–6]. Experimentally, their spin is directly accessible through the polarization of the condensate emission (Supplementary Information Section 1), enabling phenomena such as non-local spin-switching[3], multi-stability[4,14] and the optical spin-Hall effect[15]. However, while electrical control of electron spins in the solid state has greatly advanced in recent years, allowing their fully integrated injection, manipulation and detection[16], no such advances have been made regarding polaritons.

Here we demonstrate electrical control of the spin of polariton condensates. Spatially separating the condensate from its non-resonant pump (in a trapped geometry, Fig. 1b) diversifies the observed spin configurations, accessing circularly to linearly polarized states[17]. The condensate polarization depends critically on several system parameters, including tiny energetic splittings in its linear polarization. Since the latter can be tuned by electric fields, applying a bias across the microcavity provides direct control of the condensate spin. We use this mechanism to invert the spin of an optically trapped condensate exhibiting bistable behaviour, thus realizing an electrical spin-switch. Such electro-optic switching is crucial in many communications and information technology applications.

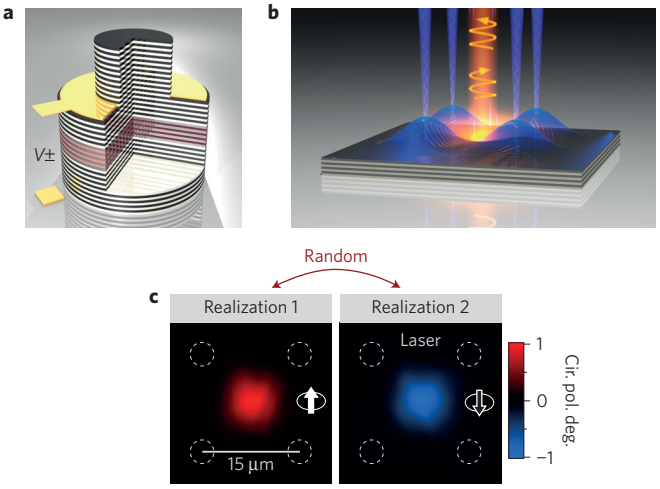

Figure 1 | Spontaneous spin polarization of trapped polariton condensates. a, Microcavity structure with 12 QWs sandwiched between two multilayer mirrors. Contacts are deposited on an etched annular recess and below the bottom reflector to apply fields perpendicular to the QW plane. *V* is the bias. **b**, Schematic of trapped polariton condensate. Four linearly polarized laser beams induce a reservoir distribution corresponding to a square-shaped potential trap (vertical axis is energy). The resulting condensate is confined to the centre and shows circular polarization. **c**, Polarization-resolved spatial images of the circular component of condensate emission for two measurements under identical experimental conditions. While both measurements exhibit strong circular polarization ($|s_z| > 95\%$), which remains stable for seconds, the direction of polarization spontaneously changes from right- (spin-up) to left-circular (spin-down) when the condensate is re-initialized. White arrows indicate condensate spin. Cir. pol. deg., degree of circular polarization.

[1]NanoPhotonics Centre, Department of Physics, Cavendish Laboratory, University of Cambridge, Cambridge CB3 0HE, UK. [2]Instituto de Energías Renovables, Universidad Nacional Autónoma de México, Temixco, Morelos 62580, Mexico. [3]CCQCN, Department of Physics, University of Crete, 71003 Heraklion, Crete, Greece. [4]Foundation for Research and Technology—Hellas, Institute of Electronic Structure and Laser, 71110 Heraklion, Crete, Greece. [5]Department of Materials Science and Technology, University of Crete, 71003 Heraklion, Crete, Greece. *e-mail: jjb12@cam.ac.uk

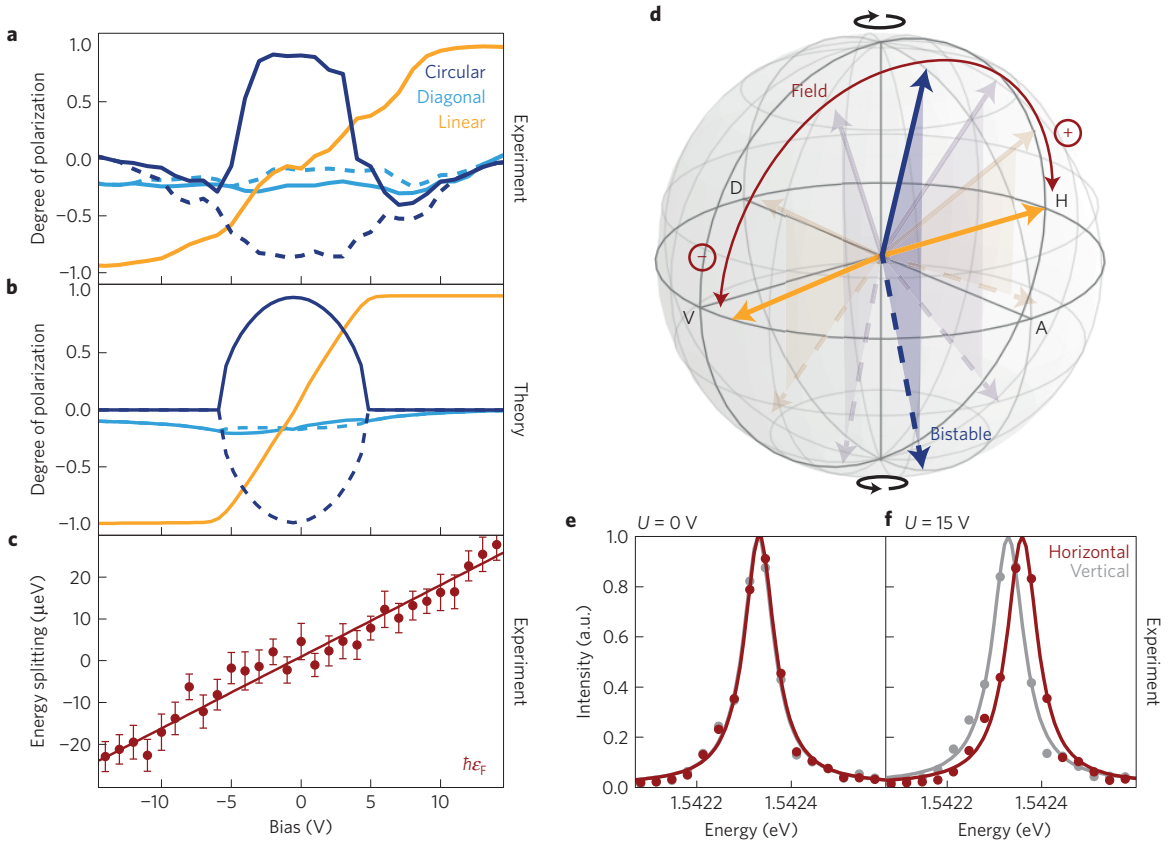

Figure 2 | Condensate polarization under external electric fields. a, Experimental bias dependence of polarization components of a trapped polariton condensate. Shown is the average polarization of bistable spin-up (solid lines) and spin-down (dashed lines) states obtained from 100 realizations at each bias, positive values for horizontal, diagonal and right-circular polarizations. **b**, Numerical simulations of the case equivalent to **a**. **c**, Measured energy splitting between horizontal–vertical condensate components versus applied bias U. Data points average 100 measurements at each bias. Linear fit gives $\hbar\epsilon_F \approx 0.9\,\mu\text{eV}\,\text{V}^{-1} \times U + 1.3\,\mu\text{eV}$. The $\hbar\epsilon_S \approx 1.3\,\mu\text{eV}$ offset at 0 V is attributed to the local effect of strain[25,26]. The error bars represent the standard error of the mean. **d**, Illustration of transition from the bistable regime at 0 V (blue) to the linear-polarized condensate at ±15 V (yellow) on the Poincaré sphere. H, V, D and A are horizontal, vertical, diagonal and anti-diagonal polarization degrees. **e**,**f**, Condensate emission spectra of horizontal and vertical components at 0 V and 15 V, showing $\hbar\epsilon_F \approx 0\,\mu\text{eV}$ and 30 μeV, respectively.

Our results are obtained from micrometre-long cavities at cryogenic temperatures, which contain twelve QWs and are processed into contacted mesas, allowing application of electric fields perpendicular to the QWs (Fig. 1a and Methods). A spatial light modulator is used to project four laser spots onto the sample surface (Fig. 1b). The linearly polarized, continuous-wave pump non-resonantly generates clouds of hot excitons, which in a series of relaxation steps accumulate at the bottom of the polariton dispersion and condense. Since polaritons are blueshifted at locations of high exciton and polariton densities due to their repulsive interactions[7], the laser pattern induces a square-shaped potential trap (Fig. 1b). Such conditions favour the formation of 'trapped' condensates which minimally overlap with the exciton reservoir, resulting in narrower linewidths and strongly reduced condensation thresholds[18–20]. Moreover, separating condensate and reservoirs leads to spontaneous breaking of the spin symmetry for excitation powers above a spin-bifurcation threshold[17]. The condensate then spontaneously adopts one of two circularly polarized bistable states under linear, non-resonant excitation, stochastically changing between right- and left-circular polarizations (spin-up and spin-down) for each realization of the experiment (Fig. 1c). Note that this spin bifurcation is favoured by the anisotropy of the nonlinear polariton–polariton interactions (see Supplementary Equation (3) and Supplementary Information Section 1) and differs fundamentally from conventional polariton bistability, where the spectral position and pump power of a resonant laser deterministically select one of the polarization states[4,14].

The influence of external electric fields on the spin of a trapped polariton condensate is explored in Fig. 2a,d. The strong circular polarization observed at 0 V transforms to elliptical as the applied bias increases, until the bistable states collapse into a single linearly polarized mode around ±15 V. The orientations of the linear polarization axes, referred to as horizontal and vertical, do not depend on the optical trap or the position on the sample surface, but are fixed along the [110] and [1$\bar{1}$0] axes of the crystal structure. The applied bias U induces a small energy splitting $\hbar\epsilon_F$ between the horizontally and vertically polarized modes, varying linearly with the bias (Fig. 2c,e,f). Two physical mechanisms contribute to this behaviour: first, applying an electric field along the [001] axis of the crystal induces birefringence due to the Pockels effect, leading to splitting of the photonic modes linearly polarized along the [110] and [1$\bar{1}$0] axes[21]. Second, external fields mix heavy- and light-hole QW excitons, lifting the degeneracy of the exciton ground state[22,23]. Both effects split linearly polarized polariton modes through a linear dependence on the external field with magnitudes matching the experimental data[21,23]. Note that the splitting between transverse electric (TE) and transverse magnetic (TM) energy observed for polaritons at larger in-plane wavevectors vanishes at normal incidence, and consequently plays no role here. Moreover, TE–TM splitting does not break the spin symmetry, and thus cannot account for the stochastic formation of circularly polarized condensates.

To interpret the experimental results, we extend the model of spontaneous spin bifurcations[17,24] to include the effects of an

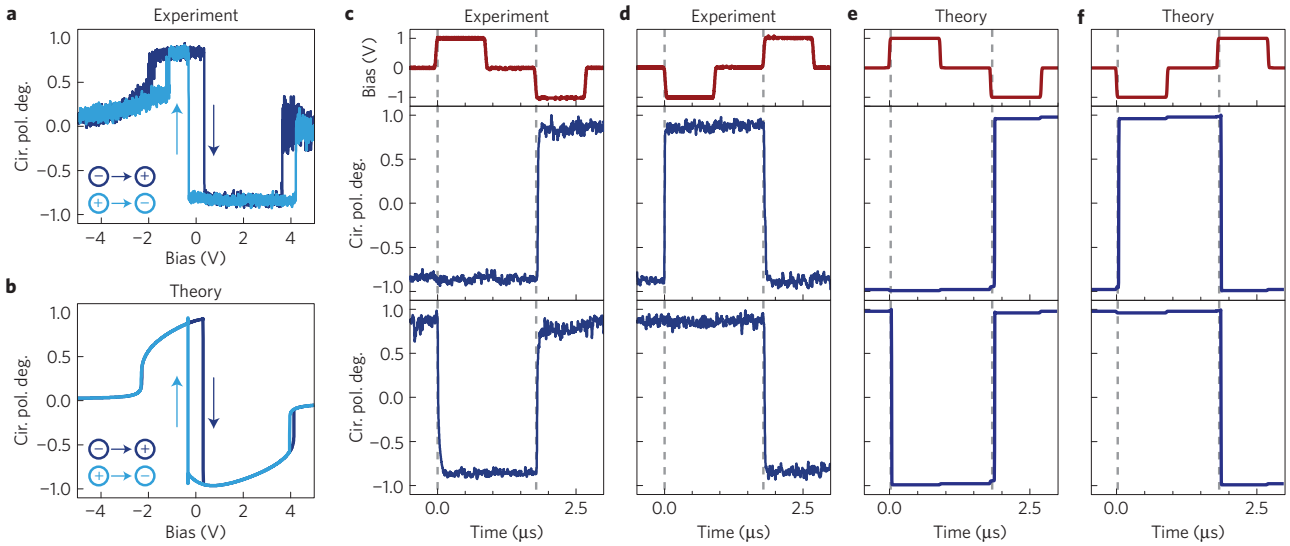

Figure 3 | Polarization hysteresis and electrical spin-switching. a, Circular polarization versus applied bias under continuous excitation. Bias swept from −5 V to +5 V (dark blue) and back (light blue) over 40 μs duration. Positive values represent right-circular polarization. **b**, Numerical simulation of **a** with an additional bias-dependent pump imbalance ΔP in the model (Supplementary Information Section 3). **c**,**d**, Experimental time evolution of circular polarization (dark blue) for ±1 V electrical pulses of 0.9 μs duration (red, top panel) acting on condensates randomly initialized in the up-states (bottom panel) and down-states (middle panel). **e**,**f**, Corresponding numerical simulations based on the model of **b**. Dashed lines mark points where the bias changes. Note: data obtained for excitation conditions different from those in Fig. 2 (see Methods).

external electric field (see Methods and Supplementary Information Section 1). A small energy splitting $\hbar\epsilon$ between two linearly polarized modes with difference -2γ between their respective loss rates induces a dynamical instability, driving a parity-breaking bifurcation above a critical density. Physically, the observed linear anisotropies $\hbar\epsilon_F$ and $\hbar\epsilon_S$ arise due to the combined effects of electric field and strain[21–23,25,26], and necessarily translate into linewidth differences $\hbar\gamma_{F,S}$ between the corresponding linear modes due to curvature of the cavity stopband (Supplementary Information Section 2). For the given microcavity structure, transfer matrix simulations predict $\gamma_{F,S} \approx 0.05\epsilon_{F,S}$, below the resolution of our experiment. Numerical simulations of Supplementary Equation (4) (Supplementary Information Section 1) are based on the measured bias dependence of $\hbar\epsilon_{F,S}$ (Fig. 2b). The good qualitative agreement with the experiment demonstrates that electrical control of the condensate spin is indeed achieved by tuning the linearly polarized condensate modes. Our model furthermore implies that the ability to bias-tune the condensate polarization depends critically on the nonlinear polariton self-interactions, which control the transition between the bistable and the linear regime (Supplementary Information Section 1).

We now realize an electrical spin-switch based on these phenomena. Slightly rotating the linear pump with respect to the crystal axes induces field-dependent birefringence (Pockels effect), giving rise to a small degree of circular polarization in the excitation. The imbalance of the left- and right-circular pump rates results in preferential occupation of one of the two bistable condensate states when applying electric fields, leading to stable left-/right-circular polarization above ±0.3 V, respectively (Fig. 3a). Under continuous optical excitation, the condensate circular polarization now exhibits hysteresis with applied voltage, corresponding to a bias threshold for spin-switching. To reproduce the experimental data, a field-dependent pump imbalance, ΔP, between the spin-up and -down components of the condensate is introduced to the model (Methods and Supplementary Information Section 3), leading to a collapse of the bistable region above ±0.3 V as well as polarization hysteresis in the numerical simulations (Fig. 3b). The system can be widely tuned, through excitation power (bistability range), sample position (rotating the axis of strain-induced splitting) and polarization of the excitation laser (spin population imbalance).

The hysteretic nature of the system allows the implementation of electrically controlled directional spin-switching (Fig. 3c,d). Electric pulses of ±1 V are applied to condensates which are randomly initialized in the bistable region, inducing switching depending on the previous condensate polarization. For instance, Fig. 3c illustrates that a +1 V pulse will only switch the spin of a condensate initialized in the right-circularly polarized state, whereas the opposite holds for a −1 V pulse. Note that the condensate state persists after the voltage pulse ends, demonstrating the bistable nature of the system. Unlike conventional switches where an energy barrier controls transitions between states, switching of this nonlinear system is achieved by temporarily destabilizing one of the basins of attraction due to the field-induced pump imbalance (Fig. 4). The measured switching time $t_s \approx 3.0$ ns is limited by our resolution (Fig. 5) and is below the rise time of the electric pulse, illustrating that the switching process is non-adiabatic.

To estimate the switching energy E_s, ±3 V electrical pulses of $t_p \approx 4.4$ ns duration are applied to the sample (Fig. 5). While switching is already observed at applied fields as low as ±0.3 V (Fig. 3a), increasing the bias significantly improves the reliability of the switching process (Supplementary Information Section 4). The current drawn $I_s = 37$ nA obtained from the device IV-curve (Supplementary Information Section 5), results in a switching energy $E_s = V_s \times I_s \times t_p \approx 0.5$ fJ. This estimate surpasses all state-of-the-art electronic (spin-) switches[2,27–29], although all-optical polariton-based solutions with better energy efficiency exist[13,30]. However, our estimate represents only an upper bound for the fundamental minimum switching energy in this system, since wasted energy from the photocurrent is not intrinsic to switching, but stems from parasitic thermal escape of hot carriers. Already at ±0.3 V, with $I_s \approx 5.6$ nA, our switching energies are $E_s \approx 10$ aJ. Improved sample designs should reduce the current drawn to the corresponding dark current (∼1.6 nA), resulting in significantly lower switching energies (Supplementary Information Section 5). The spin-switch eye diagram at applied fields of ±3 V is fully open, confirming stable operation for hundreds of cycles (Supplementary Information Section 4).

In conclusion, we demonstrate the ability to electrically control the spin of a trapped polariton condensate and realize an

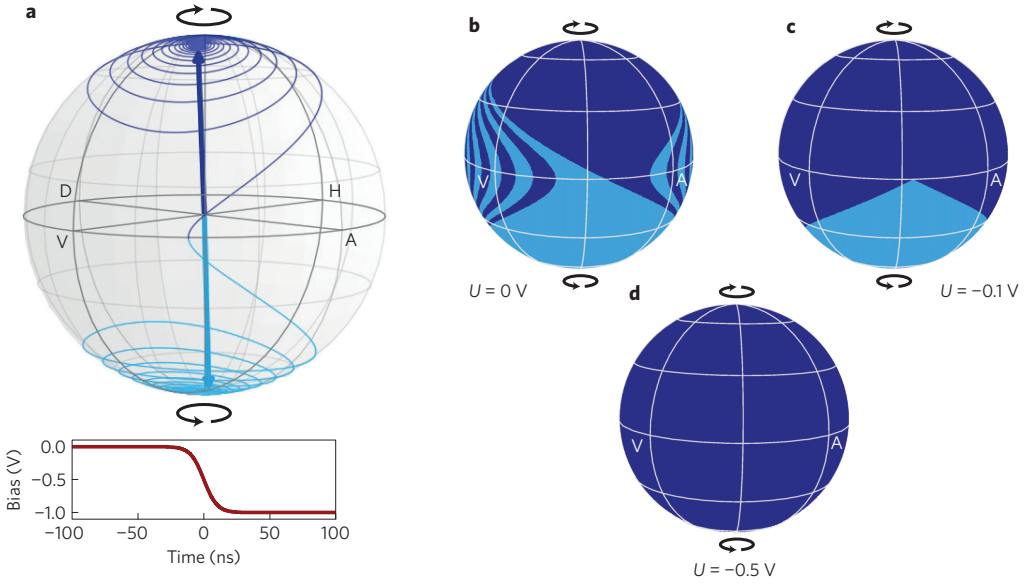

Figure 4 | Mechanism of the electrical spin-switch. a, Simulation of a switching pseudospin trajectory (from Fig. 3f middle panel, for the first switching process). **b**, Time evolution of 500 randomly chosen polarization states without applied electric field, depicted on the Poincaré sphere. Colours encode trajectories ending in the spin-up (dark blue) and spin-down (light blue) attractors, thus approximating the respective basins of attraction. **c**,**d**, Same as **b**, but for external fields of −0.1 V and −0.5 V, respectively. Simulations demonstrate how the basin of attraction of the spin-down state is destabilized due to the applied bias (see Supplementary Information Section 3 for additional discussions).

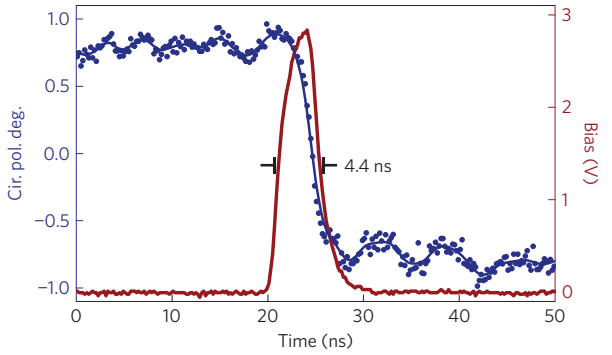

Figure 5 | Spin-switching time. Measured time evolution of the circular polarization (blue) when triggered with a 3 V bias pulse (red). Duration of the bias pulse t_p is 4.4 ns (full-width at half-maximum), while the observed condensate switching time $t_s \approx 3.0$ ns is limited by the experimental time resolution. Solid blue line is a guide to the eye.

electrical spin-switch operating at ultralow switching energies. The switching mechanism is highly reliable and the selected condensate states remain stable for many seconds (Supplementary Information Section 6). Our findings suggest implementation of electrically controlled spin-optotronic devices and effects, such as polariton-spin transistors, switches and memories[23,31], which in the case of large-bandgap materials could operate at room temperature[32]. Finally, from a more general point of view, our results represent the first example of electrically controlling the spin of a macroscopic quantum state, such as Bose–Einstein condensates or superconductors.

Methods

Methods, including statements of data availability and any associated accession codes and references, are available in the online version of this paper.

Received 24 September 2015; accepted 6 July 2016; published online 8 August 2016

References

1. Wolf, S. A. *et al*. Spintronics: a spin-based electronics vision for the future. *Science* **294,** 1488–1495 (2001).
2. Reed, G. T., Mashanovich, G., Gardes, F. Y. & Thomson, D. J. Silicon optical modulators. *Nature Photon.* **4,** 518–526 (2010).
3. Amo, A. *et al*. Exciton–polariton spin switches. *Nature Photon.* **4,** 361–366 (2010).
4. Paraïso, T. K., Wouters, M., Léger, Y., Morier-Genoud, F. & Deveaud-Plédran, B. Multistability of a coherent spin ensemble in a semiconductor microcavity. *Nature Mater.* **9,** 655–660 (2010).
5. Armitage, A. *et al*. Exciton polaritons in semiconductor quantum microcavities in a high magnetic field. *Phys. Rev. B* **55,** 16395–16403 (1997).
6. Sturm, C. *et al*. Nonequilibrium polariton condensate in a magnetic field. *Phys. Rev. B* **91,** 155130 (2015).
7. Wertz, E. *et al*. Spontaneous formation and optical manipulation of extended polariton condensates. *Nature Phys.* **6,** 860–864 (2010).
8. Nelsen, B. *et al*. Dissipationless flow and sharp threshold of a polariton condensate with long lifetime. *Phys. Rev. X* **3,** 041015 (2013).
9. Kasprzak, J. *et al*. Bose–Einstein condensation of exciton polaritons. *Nature* **443,** 409–414 (2006).
10. Balili, R., Hartwell, V., Snoke, D., Pfeiffer, L. & West, K. Bose–Einstein condensation of microcavity polaritons in a trap. *Science* **316,** 1007–1010 (2007).
11. Sanvitto, D. *et al*. Persistent currents and quantized vortices in a polariton superfluid. *Nature Phys.* **6,** 527–533 (2010).
12. Gao, T. *et al*. Polariton condensate transistor switch. *Phys. Rev. B* **85,** 235102 (2012).
13. Ballarini, D. *et al*. All-optical polariton transistor. *Nature Commun.* **4,** 1778 (2013).
14. Cerna, R. *et al*. Ultrafast tristable spin memory of a coherent polariton gas. *Nature Commun.* **4,** 2008 (2013).
15. Leyder, C. *et al*. Observation of the optical spin Hall effect. *Nature Phys.* **3,** 628–631 (2007).
16. Awschalom, D. D. & Flatté, M. E. Challenges for semiconductor spintronics. *Nature Phys.* **3,** 153–159 (2007).
17. Ohadi, H. *et al*. Spontaneous spin bifurcations and ferromagnetic phase transitions in a spinor exciton–polariton condensate. *Phys. Rev. X* **5,** 031002 (2015).
18. Cristofolini, P. *et al*. Optical superfluid phase transitions and trapping of polariton condensates. *Phys. Rev. Lett.* **110,** 186403 (2013).
19. Dreismann, A. *et al*. Coupled counterrotating polariton condensates in optically defined annular potentials. *Proc. Natl Acad. Sci. USA* **111,** 8770–8775 (2014).

20. Askitopoulos, A. *et al*. Polariton condensation in an optically induced two-dimensional potential. *Phys. Rev. B* **88,** 041308 (2013).
21. Park, M. S. *et al*. Polarization control of vertical-cavity surface-emitting lasers by electro-optic birefringence. *Appl. Phys. Lett.* **76,** 813–815 (2000).
22. Aleiner, I. L. & Ivchenko, E. L. Anisotropic exchange splitting in type-II GaAs/AlAs superlattices. *J. Exp. Theor. Phys.* **55,** 692–695 (1992).
23. Malpuech, G., Glazov, M. M., Shelykh, I. A., Bigenwald, P. & Kavokin, K. V. Electronic control of the polarization of light emitted by polariton lasers. *Appl. Phys. Lett.* **88,** 111118 (2006).
24. Aleiner, I. L., Altshuler, B. L. & Rubo, Y. G. Radiative coupling and weak lasing of exciton–polariton condensates. *Phys. Rev. B* **85,** 121301 (2012).
25. Kłoptowski, L. *et al*. Optical anisotropy and pinning of the linear polarization of light in semiconductor microcavities. *Solid State Commun.* **139,** 511–515 (2006).
26. Balili, R. *et al*. Huge splitting of polariton states in microcavities under stress. *Phys. Rev. B* **81,** 125311 (2010).
27. Wada, O. Femtosecond all-optical devices for ultrafast communication and signal processing. *New J. Phys.* **6,** 183 (2004).
28. Nozaki, K. *et al*. Sub-femtojoule all-optical switching using a photonic-crystal nanocavity. *Nature Photon.* **4,** 477–483 (2010).
29. Fiori, G. *et al*. Electronics based on two-dimensional materials. *Nature Nanotech.* **9,** 768–779 (2014).
30. Marsault, F. *et al*. Realization of an all optical exciton–polariton router. *Appl. Phys. Lett.* **107,** 201115 (2015).
31. Shelykh, I. A., Johne, R., Solnyshkov, D. D. & Malpuech, G. Optically and electrically controlled polariton spin transistor. *Phys. Rev. B* **82,** 153303 (2010).
32. Christmann, G., Butté, R., Feltin, E., Carlin, J.-F. & Grandjean, N. Room temperature polariton lasing in a GaN/AlGaN multiple quantum well microcavity. *Appl. Phys. Lett.* **93,** 051102 (2008).

Acknowledgements

We acknowledge grants EPSRC EP/L027151/1, EU INDEX 289968, ERC "POLAFLOW" Starting grant, ERC LINASS 320503, Spanish MEC (MAT2008-01555), Mexican CONACYT 251808, EU FP7-REGPOT-2013-1 grant agreement 316165 II, Leverhulme Trust Grant No. VP1-2013-011 and Fundación La Caixa. We thank B. de Nijs for discussions.

Author contributions

A.D., H.O., Z.H., P.G.S. and J.J.B. designed the research. A.D., H.O., Y.d.V.-I.R. and R.B. performed experiments. A.D., H.O., Y.d.V.-I.R. and Y.G.R. performed theoretical analysis and numerical simulations. S.I.T., G.D., Z.H. and P.G.S. managed the design and growth of samples. A.D., H.O., Y.d.V.-I.R. and J.J.B. analysed data. A.D., H.O. and J.J.B. wrote the paper.

Additional information

Supplementary information is available in the online version of the paper. Reprints and permissions information is available online at www.nature.com/reprints. Correspondence and requests for materials should be addressed to J.J.B.

Competing financial interests

The authors declare no competing financial interests.

Methods

Sample. The sample studied is a $5\lambda/2$ $Al_{0.3}Ga_{0.7}As$ microcavity, formed by distributed Bragg reflectors (DBRs) with 32/35 layer pairs on top/bottom. The individual layer pairs are composed of $Al_{0.15}Ga_{0.85}As$/AlAs with thicknesses of 57.2/65.4 nm, respectively. The quality factor of the microcavity exceeds $Q > 16{,}000$. Four sets of three GaAs QWs are located at the maxima of the light field in the cavity, resulting in a exciton–photon Rabi-splitting of 9.2 meV. The cavity mode is detuned approximately −5 meV relative to the exciton energy. The 200-μm-diameter mesas are etched into the sample and electrical contacts deposited on the *n*-doped substrate and on an annular recess around the top of the mesa, four DBR layers above the cavity location. An applied bias U provides a resulting electric field $F\ [\mathrm{kV\,cm^{-1}}] \approx 1.86\,\mathrm{cm^{-1}} \times U\ [\mathrm{V}]$.

Experimental techniques. Polaritons are excited non-resonantly, with a horizontally polarized, single-mode continuous-wave laser (wavelength $\lambda = 750$ nm) at a total power of approximately 40 mW in four separate spots. The excitation amplitude is modulated with an acousto-optic modulator giving a rise time of 90 ns. A spatial light modulator is employed to generate patterns of laser spots on the sample surface. The resulting emission around 800 nm is polarization resolved with a series of beam splitters, quarter- and half-waveplates and a Wollaston prism to simultaneously measure its linear, diagonal and circular components. The signal is recorded with a charge-coupled device (CCD) for imaging and a monochromator plus CCD for spectral analysis, while photomultipliers are employed for measurements with a time resolution of 7 ns. A source-measurement unit is used to apply fields across the sample and monitor the resulting currents. All measurements were performed at cryogenic temperatures ($T < 10$ K). For further details see ref. 33.

Theoretical description. Simulations of Figs 2b, 3e,f and 4 are based on equations of the form (see Supplementary Information Section 1 and 3 for a detailed discussion):

$$i\dot{\Psi} = -\frac{i}{2}g(S)\Psi - \frac{i}{2}(a_S\sigma_x + b_S\sigma_y)(\gamma_S - i\epsilon_S)\Psi - \frac{i}{2}(a_F\sigma_x + b_F\sigma_y)(\gamma_F - i\epsilon_F)\Psi + \frac{1}{2}[(\alpha_1+\alpha_2)S + (\alpha_1-\alpha_2)S_z\sigma_z]\Psi \quad (1)$$

where $\hbar$ was set to 1 and $\Psi = (\psi_+, \psi_-)^{\mathrm{T}}$ is the condensate order parameter with ψ_+ and ψ_- the spin-up and spin-down components. The factor $g(S)$ describes the balance between the pump rate P and the decay rate Γ, with $g(S) = \Gamma - P + \eta S$. The term ηS accounts for gain saturation, with the total occupation $2S = |\psi_-|^2 + |\psi_+|^2$ and the saturation factor η. In the case of an imbalanced pump, $g(S)$ takes the form $g(S) = (\Gamma - (1-\beta)P + \eta S, \Gamma - (1+\beta)P + \eta S)^{\mathrm{T}}$, with the field-induced pump imbalance $\Delta P = 2\beta(F)P$ (see Supplementary Information Section 3 for details). The factors $\epsilon_{S,F}$ and $\gamma_{S,F}$ denote the energy splitting and corresponding linewidth differences arising from sample strain and an applied electric field, respectively. The splitting axis is selected by the factors $a_{S,F}$ and $b_{S,F}$, where $a_i^2 + b_i^2 = 1$ and $a_i, b_i \in [-1, 1]$. The coefficients α_1 and α_2 represent the strength of same- and cross-spin polariton–polariton interactions and $\sigma_{x,y,z}$ are the Pauli matrices.

Numerical simulations. The parameters used for the numerical simulations of Fig. 2b and Supplementary Information Section 1 are: $\eta = 0.01\ \mathrm{ps^{-1}}$, $\Gamma = 0.2\ \mathrm{ps^{-1}}$, $P = 0.205\ \mathrm{ps^{-1}}$, $\hbar\alpha_1 = 10\,\mu\mathrm{eV}$ and $\alpha_2 = -0.5 \times \alpha_1$. The field-induced energy splitting $\hbar\epsilon_F$ as a function of the applied bias U is determined from the linear fit in Fig. 2c as $\hbar\epsilon_F \approx 0.9\,\mu\mathrm{eV}/V \times U + 1.3\,\mu\mathrm{eV}$. The offset of $\hbar\epsilon_F$ is attributed to the effect of strain, with a maximum field-independent splitting $\hbar\epsilon_S \approx 1.6\,\mu\mathrm{eV}$ being observed along the axes rotated by −25° relative to the horizontal/vertical ($a_S = -0.6$). The corresponding linewidth differences are derived from the transfer matrix calculations presented in Supplementary Information Section 2 as $\gamma_{S,F} = 0.05 \times \epsilon_{S,F}$. To achieve a better fit of the diagonal polarization at large fields, the linear polarization axes between which the splitting $\hbar\epsilon_F$ is induced are assumed to be rotated by 1.3° with respect to the experimentally defined horizontal and vertical axes—that is, $a_F = 0.999$.

The data presented in Fig. 3 were obtained at a sample position (different strain) and excitation power different from those used in Fig. 2, with the corresponding parameters being changed to $P = 0.203\ \mathrm{ps^{-1}}$ and $a_S = 0.6$ to match the experimental data. Additionally, a field-dependent imbalance ΔP was added to the pump terms of the spin-up and -down components, with $\Delta P = \mp U \times P \times 0.002$. The same parameters were used for the simulations in Supplementary Information Section 3 and 5.

Data availability. Source data can be found at: http://dx.doi.org/10.17863/CAM.748.

References

33. Tsotsis, P. *et al*. Tuning the energy of a polariton condensate via bias-controlled Rabi splitting. *Phys. Rev. Appl.* **2,** 014002 (2014).